

# Synthesis, Characterization, and DFT Studies of *N*-(3,5-Bis(trifluoromethyl)benzyl)stearamide

Angélica Salinas-Torres, Hugo Rojas, José J. Martínez , Diana Becerra \*  and Juan-Carlos Castillo \* 

Grupo de Catálisis de la UPTC, Escuela de Ciencias Química, Facultad de Ciencias, Universidad Pedagógica y Tecnológica de Colombia, Avenida Central del Norte 39-115, Tunja 150003, Colombia; angelica.salinas@uptc.edu.co (A.S.-T.); hugo.rojas@uptc.edu.co (H.R.); jose.martinez@uptc.edu.co (J.J.M.)

\* Correspondence: diana.becerra08@uptc.edu.co (D.B.); juan.castillo06@uptc.edu.co (J.-C.C.);

Tel.: +57-8-740-5626 (ext. 2425) (D.B. & J.-C.C.)

**Abstract:** The novel *N*-(3,5-bis(trifluoromethyl)benzyl)stearamide **3** was prepared in moderate yield by a solventless direct amidation reaction of stearic acid **1** with 3,5-bis(trifluoromethyl)benzylamine **2** at 140 °C for 24 h under metal- and catalyst-free conditions. This practical method was conducted in air without any special treatment or activation. The fatty acid amide **3** was fully characterized by IR, UV-Vis, 1D and 2D NMR spectroscopy, mass spectrometry, and elemental analysis. Moreover, molecular electrostatic potential studies, determination of quantum descriptors, fundamental vibrational frequencies, and intensity of vibrational bands were computed by density functional theory (DFT) using the B3LYP method with 6-311+G(d,p) basis set in gas phase. Simulation of the infrared spectrum using the results of these calculations led to good agreement with the observed spectral patterns.

**Keywords:** solventless direct amidation; nonactivated carboxylic acid; benzylamine derivative; fatty acid amide; DFT quantum-chemical studies



**Citation:** Salinas-Torres, A.; Rojas, H.; Martínez, J.J.; Becerra, D.; Castillo, J.-C. Synthesis, Characterization, and DFT Studies of *N*-(3,5-Bis(trifluoromethyl)benzyl)stearamide. *Molbank* **2021**, *2021*, M1215. <https://doi.org/10.3390/M1215>

Academic Editor: Ian R. Baxendale

Received: 18 May 2021  
Accepted: 24 May 2021  
Published: 25 May 2021

**Publisher's Note:** MDPI stays neutral with regard to jurisdictional claims in published maps and institutional affiliations.



**Copyright:** © 2021 by the authors. Licensee MDPI, Basel, Switzerland. This article is an open access article distributed under the terms and conditions of the Creative Commons Attribution (CC BY) license (<https://creativecommons.org/licenses/by/4.0/>).

## 1. Introduction

The amide bond is one of the most important and fascinating functional groups in organic chemistry and biochemistry owing to its widespread occurrence in natural products, peptides, proteins, and a plethora of other biomolecules [1,2]. Medicinally, the amide-forming reactions are pivotal in the pharmaceutical industry and medicinal chemistry for the preparation of active pharmaceutical ingredients [3,4], insecticides [5,6], polymers [7], and a vast number of bioactive molecules [8–12]. Most notably, the amide functional group is present in approximately a quarter of clinically approved drugs and two-thirds of all drug candidates [13]. In particular, the fatty acid amides (FAAs) have received augmented interest due to their wide range of physiological and pharmacological activities. Members of FAAs include the *N*-acyltaurines such as *N*-arachidonoyltaurine that activates TRPV1 and TRPV4 calcium channels of the kidney [14]; the *N*-acylethanolamines (NAEs) such as *N*-arachidonoylethanolamine (anandamide), an endogenous ligand for the cannabinoid CB1 and CB2 receptors in the mammalian brain [15,16]; the *N*-acylamino acids (NAAs) such as *N*-arachidonylglycine that suppresses pain via a peripheral action [17]; and the primary fatty acid amides (PFAMs) such as oleamide that shows an important therapeutic potential in the management of sleep disorders and pain [18,19], as illustrated in Figure 1.

The procedures most used in the pharmaceutical industry for amide synthesis involve the acylation reaction of activated carboxylic acid derivatives such as acyl chlorides, anhydrides, or esters with amines, as well as the direct amidation of carboxylic acids with amines employing stoichiometric quantities of diverse coupling reagents, which generate large quantities of waste leading to poor atom-economy and tricky purification procedures [20–22]. Hence, in the past two decades, there was a significant increase in

the development of sustainable catalytic methods for amide bond formation under mild conditions with a broad synthetic scope [23–26]. In particular, we recently reported a solventless direct amidation of non-activated carboxylic acids with amines employing a biogenic CuO–CaCO<sub>3</sub> catalyst for amide synthesis in moderate to high yields under normal atmospheric conditions [27]. Despite the elegant progress that has been accomplished, most catalytic direct amidation methods are unattractive for large-scale production owing to the limited substrate scope, low energy efficiency, poor sustainability, and not industrially relevant levels of recyclability of most current catalysts [23,24]. Importantly, the metal- and catalyst-free direct amidation of carboxylic acids with amines has been neglected for many years owing to its high temperatures and long reaction times; nonetheless, this thermal approach can eliminate some of the previously reported synthetic drawbacks. In connection with the ongoing development of efficient and simple protocols for the construction of carbon–nitrogen bonds [27–31] and our current studies on the synthetic utility of benzylamine derivatives [32,33], we describe a solventless synthesis of *N*-(3,5-bis(trifluoromethyl)benzyl)stearamide **3** through an uncatalyzed process under normal atmospheric conditions. Moreover, molecular electrostatic potential studies, determination of quantum descriptors, fundamental vibrational frequencies, and intensity of vibrational bands were computed by the B3LYP method using 6–311+G(d,p) basis set in gas phase.

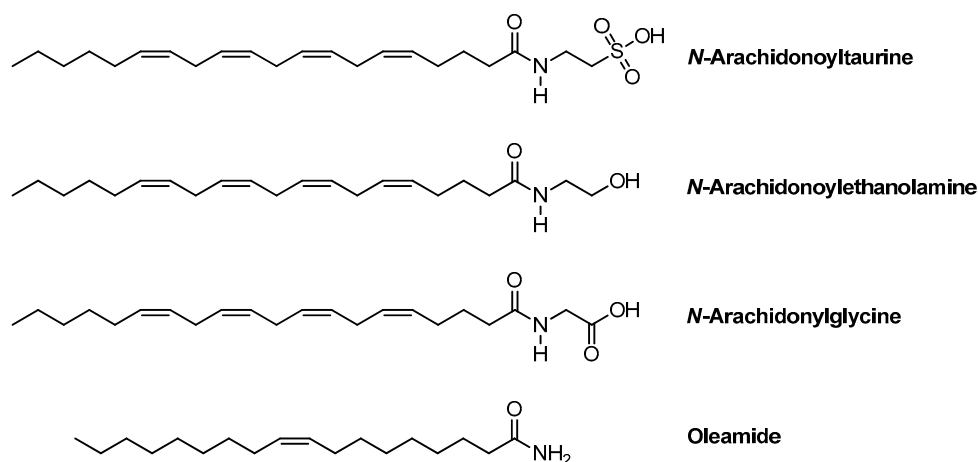


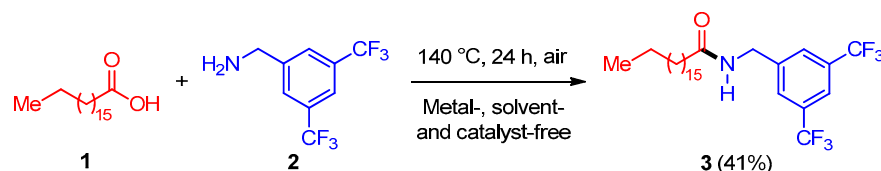
Figure 1. Bioactive amides of fatty acids.

## 2. Results and Discussion

### 2.1. Synthesis

We report a metal- and catalyst-free synthesis of *N*-(3,5-bis(trifluoromethyl)benzyl)stearamide **3** by a direct amidation reaction between equimolar amounts of stearic acid **1** with 3,5-bis(trifluoromethyl)benzylamine **2** at 140 °C for 24 h under solvent-free conditions, as depicted in Scheme 1. It should be noted that the water vapor condensed on the walls of the open-topped tube was removed with a small piece of cotton attached to a spatula to displace the equilibrium towards amide formation. After the specified reaction time, the mixture was allowed to cool to ambient temperature, and the resulting crude product was purified by flash chromatography on silica gel using a mixture of DCM/MeOH (100:1, *v/v*) as eluent to furnish the fatty acid amide **3** in 41% yield. Conceptually, the condensation reaction between a carboxylic acid and an amine is the most attractive and practical synthetic approach to form the amide bond via the expulsion of a molecule of water. Nonetheless, the amide **3** was isolated in moderate yield (41%) because the innate acidity of the stearic acid and the basicity of the 3,5-bis(trifluoromethyl)benzylamine can generate ionized forms that limit its thermal condensation. Despite the moderate yield, the collateral formation of substituted ammonium carboxylate salt was not detected by thin-layer chromatography (TLC) and <sup>1</sup>H NMR spectroscopy. In consequence, the releasing

of water as the unique by-product gives to this approach a remarkable eco-friendly quality. It should be noted that the synthesis and full characterization of amide **3** have not been reported on Reaxys and SciFinder databases. For that reason, a full spectroscopic and analytical characterization was performed in this work (see Section 3 and Figures S1–S5). The IR, 1D NMR, and MS spectra and elemental analysis suggest that the structure of the isolated white solid corresponds to the amide **3**. Furthermore, 2D HSQC, HMBC, and COSY experiments permit the assignment of all proton and carbon atoms, confirming the proposed structure for amide **3** without ambiguity (see Supplementary Material).



**Scheme 1.** Solventless synthesis of *N*-(3,5-bis(trifluoromethyl)benzyl)stearamide **3** by a metal- and catalyst-free direct amidation.

The  $^1\text{H-NMR}$  spectrum recorded in deuterated chloroform using TMS as internal standard showed 35 protons in the range of 0.86–2.28 ppm assigned to the long aliphatic chain, a doublet at 4.56 ( $J = 6.4$  Hz) ppm attributed to  $\text{CH}_2\text{N}$  protons, a triplet at 6.02 ( $J = 5.6$  Hz) assigned to the NH proton, two singlets at 7.72 and 7.78 ppm associated with aromatic protons, and the absence of COOH and  $\text{NH}_2$  protons, indisputably confirming the thermal direct amidation of fatty acid **1** with benzylamine derivative **2**. The presence of 1 methyl carbon at 14.3 ppm, 17 different types of methylene carbons in the range of 22.8–42.7 ppm, 2 methinic carbons at 121.5 ( $^3J_{\text{C-F}} = 4.0$  Hz) and 127.8 ( $^3J_{\text{C-F}} = 3.0$  Hz) ppm, and 4 quaternary carbons involving  $\text{CF}_3$  and  $\text{C=O}$  functionalities at 123.3 ( $^1J_{\text{C-F}} = 274.0$  Hz) and 173.6 ppm, respectively, are the most relevant features of the  $^{13}\text{C}\{^1\text{H}\}$  NMR spectrum. As expected, some aromatic carbons appeared as quartets with intensities 1:3:3:1 due to the splitting caused by the fluorine atoms on trifluoromethyl groups attached to the benzene ring. A molecular ion with  $m/z$  509 in the mass spectrum is also consistent with the structure **3**. Ultimately, two well-defined absorptions are noted in the UV–Vis spectrum recorded in acetonitrile at 205.0 and 265.7 nm corresponding to  $\pi \rightarrow \pi^*(\text{C=O})$  and  $n \rightarrow \pi^*(\text{C=O})$  transitions, respectively (see Supplementary Material).

## 2.2. Molecular Electrostatic Potential (MEP) Mapping

In order to study the electronic behavior of amide **3**, the geometric optimization was computed using density functional theory (DFT), employing Becke's three-parameter hybrid function with the nonlocal correlation of Lee–Yang–Parr (B3LYP) method at 6–311+G(d,p) basis set in gas phase [34,35]. The atomic coordinates of the optimized structure of **3** are given in Table S1. Afterward, the molecular electrostatic potential (MEP) was calculated to find the charge distribution on the surface of **3**, as well as to determine the sites with higher and lower electrostatic potential, as shown in Figure 2. It is important to mention that electrostatic potentials at the surface are represented by different colors, such as red, electron-rich; blue, electron-deficient; light blue, slightly electron-deficient; and yellow, slightly electron-rich. The MEP analysis for amide **3** showed an electron-rich region around the carbonyl oxygen, whereas an electron-deficient region is located around the amide nitrogen; these findings are in good agreement with the resonance hybrid contributions in amides [36]. In addition, two green regions located around both 3,5-bis(trifluoromethyl)phenyl moiety and long aliphatic chain showed potential sites for lipophilic interactions.

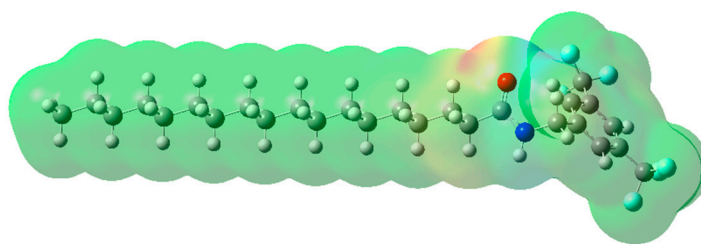


**Figure 2.** Molecular electrostatic potential mapped of amide 3.

### 2.3. Frontier Orbitals and Global Reactivity Descriptors

The frontier molecular orbitals (FMO) energy levels highest occupied molecular orbital (HOMO) and lowest unoccupied molecular orbital (LUMO) for amide 3 were computed using the B3LYP method with 6-311+G(d,p) basis set in gas phase. The HOMO and LUMO energies represent the ability to donate and gain an electron, respectively. The HOMO–LUMO energy gap and the pictorial illustration of HOMO and LUMO are shown in Figure 3. For the optimized structural models, the HOMO is located over the amide nitrogen ( $N2p_z$ ), which indicates that the majority of charge transfer occurs between amide nitrogen and carbonyl carbon, in line with the resonance model in amides [36]. Furthermore, the LUMO is mainly located over the 3,5-bis(trifluoromethyl)phenyl moiety with a minor contribution of the  $\pi^*_{C=O}$  orbital, which indicates the small contribution of carbonyl oxygen to the LUMO. As a result, the basic amide nitrogen and the acidic carbonyl group in amide 3 become less reactive, which is evidenced by the high HOMO–LUMO gap (5.54 eV).

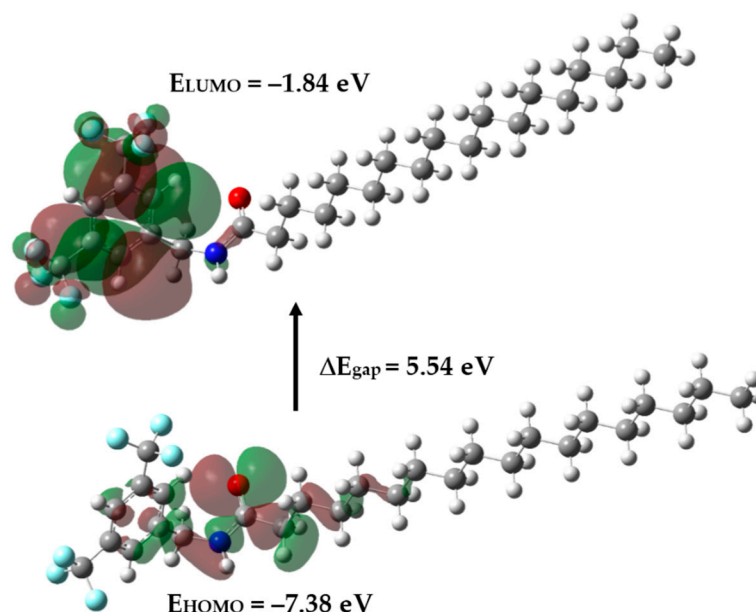


**Figure 3.** Computed energy levels HOMO–LUMO of amide 3 using the B3LYP method with 6-311+G(d,p) basis set in gas phase.

The calculated ionization potential (IP), electron affinity (EA), electrophilicity index ( $\omega$ ), chemical potential ( $\mu$ ), electronegativity ( $\chi$ ), and hardness ( $\eta$ ) for amide 3 are illustrated in Table 1. The Koopmans' theorem in density functional theory has shown that the highest occupied molecular orbital (HOMO) and the lowest unoccupied molecular orbital (LUMO) energies of typical molecules are compared with the ionization potential (IP) and electron affinity (EA), respectively [37]. The average value of HOMO and LUMO energies is related to the electronegativity ( $\chi$ ), as  $\chi = (IP + EA)/2$  [38]. The HOMO–LUMO energy gap is correlated to the hardness ( $\eta$ ), which is a good indicator of the chemical stability [39]. Parr and coworkers incorporated the term electrophilicity index ( $\omega$ ), as  $\omega = \mu^2/2\eta$  where  $\mu$  is the chemical potential taking the average value  $\mu = -(IP + EA)/2$  [40]. The negative value

of the chemical potential ( $\mu = -4.61$  eV) for amide **3** is associated with a good chemical stability resulting in a high melting point. The magnitude of the hardness ( $\eta$ ) supported by the HOMO–LUMO energy gap is 5.54 eV, indicating a low chemical reactivity. Besides, the low HOMO energy ( $-7.38$  eV) indicates the difficulty of electron donation of the amide **3** due to its high electronegativity value ( $\chi = 4.61$  eV). Electrophilicity is an important descriptor of reactivity that allows the quantitative classification of the global electrophilic nature of a molecule within a relative scale. Consequently, Domingo and coworkers established an electrophilicity ( $\omega$ ) scale for the classification of organic molecules as strong electrophiles with  $\omega > 1.5$  eV, moderate electrophiles with  $0.8 < \omega < 1.5$  eV, and marginal electrophiles with  $\omega < 0.8$  eV [38]. As shown in Table 1, the amide **3** can be regarded as a strong electrophile ( $\omega = 1.92$  eV).

**Table 1.** HOMO and LUMO orbital energies (eV) and global reactivity descriptors (eV) of amide **3**.

Parameters	Amide 3
HOMO energy	−7.38
LUMO energy	−1.84
HOMO–LUMO energy gap	5.54
Ionization potential (IP)	7.38
Electron affinity (EA)	1.84
Electrophilicity index ( $\omega$ )	1.92
Chemical potential ( $\mu$ )	−4.61
Electronegativity ( $\chi$ )	4.61
Hardness ( $\eta$ )	5.54

#### 2.4. Vibrational Analysis

For visual comparison, a superposition of experimental and calculated [B3LYP/6–311+G(d,p)] FT-IR spectra is illustrated in Figure 4. The vibrational frequencies from DFT calculations are often overestimated and commonly scaled by empirical factors. A scaling factor of 1.0 was used in this study to fit the calculated frequencies to the experimental ones. For the amide **3**, the most relevant computed scaled frequencies attributed to N–H and C=O stretching vibrations were 3642.71 and 1739.37  $\text{cm}^{-1}$ , while experimental frequencies were observed at 3290.54 and 1647.48  $\text{cm}^{-1}$ , respectively. Moreover, the computed scaled frequencies attributed to C–N–H in-plane deformation and C–N stretching vibrations were 1536.04 and 1280.41  $\text{cm}^{-1}$ , while experimental frequencies were assigned at 1557.52 and 1285.09  $\text{cm}^{-1}$ , respectively. Ultimately, absorption bands at 1174.98  $\text{cm}^{-1}$  ( $\nu_{\text{as}}$  C–F) and 1115.40  $\text{cm}^{-1}$  ( $\nu_{\text{s}}$  C–F) were observed for  $\text{CF}_3$ -containing amide **3**, while the calculated scaled vibrations were assigned at 1169.85 and 1123.66  $\text{cm}^{-1}$ , respectively.

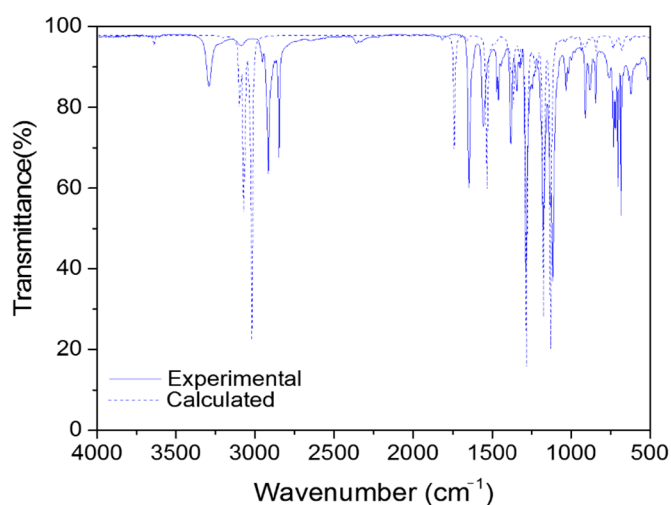


**Figure 4.** Superposition of experimental and calculated [B3LYP/6–311+G(d,p)] FT-IR spectra of amide **3**.

### 3. Materials and Methods

#### 3.1. General Information

Stearic acid and 3,5-bis(trifluoromethyl)benzylamine were purchased from Sigma-Aldrich and used without further purification. Starting materials were weighed and handled in air at ambient temperature. Silica gel aluminum plates (Merck 60 F<sub>254</sub>, Darmstadt, Germany) were used for analytical TLC. The IR absorption spectrum was recorded at room temperature from 4000 to 500 cm<sup>-1</sup> employing a Nicolet iS50 FTIR spectrometer (Thermo Fischer Scientific Inc., Madison, WI, USA) equipped with an attenuated reflectance accessory. <sup>1</sup>H and <sup>13</sup>C{<sup>1</sup>H}-NMR spectra were recorded at 25 °C on a Bruker Avance 400 spectrophotometer (Bruker BioSpin GmbH, Rheinstetten, Germany) operating at 400 and 101 MHz, respectively. The concentration of the sample was approximately 15 mg/0.6 mL of CDCl<sub>3</sub>. Chemical shifts of <sup>1</sup>H and <sup>13</sup>C{<sup>1</sup>H} NMR experiments were referenced by tetramethylsilane ( $\delta = 0.0$  ppm). Alternatively, chemical shifts of <sup>1</sup>H and <sup>13</sup>C{<sup>1</sup>H}-NMR experiments can be referenced by the residual nondeuterated signal ( $\delta = 7.26$  ppm) and the deuterated solvent signal ( $\delta = 77.16$  ppm), respectively. DEPT spectra were used for the assignment of carbon signals. Chemical shifts ( $\delta$ ) are given in ppm and coupling constants ( $J$ ) are given in Hz. The following abbreviations are used for multiplicities:  $s$  = singlet,  $d$  = doublet,  $t$  = triplet,  $q$  = quartet, and  $m$  = multiplet. 2D NMR experiments HSQC, HMBC, and COSY were performed using the standard Bruker pulse sequence. NMR data were analyzed using MestReNova 12.0.0 (2017) software. Mass spectrum was run on a SHIMADZU-GCMS 2010-DI-2010 spectrometer (Scientific Instruments Inc., Columbia, WA, USA) (equipped with a direct inlet probe) operating at 70 eV. Microanalysis was performed on a CHNS elemental analyzer (Thermo Fischer Scientific Inc., Madison, WI, USA), and the values were within  $\pm 0.4\%$  of the theoretical values. The UV-Vis absorption spectrum was obtained from an acetonitrile solution ( $5.0 \times 10^{-4}$  M) in an Evolution 201 UV-Vis spectrophotometer (Thermo Fischer Scientific Inc., Madison, WI, USA).

#### 3.2. Computational Study

The geometry optimization of the *N*-(3,5-bis(trifluoromethyl)benzyl)stearamide **3** was performed using density functional theory (DFT), employing Becke's three-parameter hybrid function with the nonlocal correlation of Lee-Yang-Parr (B3LYP) method with 6-311+G(d,p) basis set in gas phase. Theoretical calculations were performed by DFT using Gaussian 16 [34,35,41]. The molecular visualization, optimized geometry, and molecular electrostatic potential were obtained using GaussView 6.0.16. The multiwfn algorithm was used for these calculations. It should be noted that DFT calculations were performed for the prediction of chemical stability and reactivity of amide **3** with the help of quantum chemical descriptors such as frontier molecular orbitals and HOMO-LUMO energy gap, as well as global reactivity descriptors such as potential (IP), electron affinity (EA), electrophilicity index ( $\omega$ ), chemical potential ( $\mu$ ), electronegativity ( $\chi$ ), and hardness ( $\eta$ ). The molecular electrostatic potential (MEP) analysis is presented as a powerful tool for the knowledge of charge distribution, and its results can be useful in determining how amide **3** molecules could interact with each other.

#### 3.3. Synthesis of *N*-(3,5-Bis(trifluoromethyl)benzyl)stearamide **3**

A 10.0 mL open-topped tube was filled with stearic acid **1** (142 mg, 0.50 mmol, CAS 57-11-4) and 3,5-bis(trifluoromethyl)benzylamine **2** (122 mg, 0.50 mmol, CAS 85068-29-7), and the resulting mixture was heated in an oil bath at 140 °C for 24 h under solvent-free conditions. It should be noted that the water vapor condensed on the walls of the open-topped tube was removed with a small piece of cotton attached to a spatula to displace the equilibrium towards amide formation. Then, the mixture was allowed to cool to ambient temperature, and the resulting crude product was purified by flash chromatography on silica gel using a mixture of DCM/MeOH (100:1,  $v/v$ ) as eluent to afford the fatty acid amide **3** as a white solid (104 mg, 41% yield).  $R_f$  (DCM/MeOH: 50/1) = 0.70. M.p 83–85 °C. FTIR-ATR:  $\nu = 3290$  ( $\nu$  N-H), 2953, 2916, 2848, 1647 ( $\nu$  C=O,  $\nu$  C=C), 1557 ( $\delta$  N-H),

1285 ( $\nu$  C–N), 1174 ( $\nu_{as}$  C–F), 1115 ( $\nu_s$  C–F), 908, 843, 730, 684  $\text{cm}^{-1}$ . UV–Vis (acetonitrile)  $\lambda_{max}$  ( $\epsilon$ ,  $\text{L}\cdot\text{mol}^{-1}\cdot\text{cm}^{-1}$ ): 205.0 (5740,  $\pi\rightarrow\pi^*(\text{C}=\text{O})$ ), 265.7 (576,  $n\rightarrow\pi^*(\text{C}=\text{O})$ ) nm.  $^1\text{H-NMR}$  (400 MHz,  $\text{CDCl}_3$ ):  $\delta$  = 0.87 (t,  $J$  = 6.6 Hz, 3H), 1.20–1.35 (m, 28H), 1.66 (quint,  $J$  = 6.8 Hz, 2H), 2.26 (t,  $J$  = 7.6 Hz, 2H,  $\text{CH}_2\text{CO}$ ), 4.56 (d,  $J$  = 6.4 Hz, 2H,  $\text{CH}_2\text{NH}$ ), 6.02 (t,  $J$  = 5.6 Hz, 1H, NH), 7.72 (s, 2H,  $\text{H}_o$ ), 7.78 (s, 1H,  $\text{H}_p$ ) ppm.  $^{13}\text{C}\{^1\text{H}\}\text{-NMR}$  (101 MHz,  $\text{CDCl}_3$ ):  $\delta$  = 14.3 ( $\text{CH}_3$ ), 22.8 ( $\text{CH}_2$ ), 25.8 ( $\text{CH}_2$ ), 29.4 ( $\text{CH}_2$ ), 29.5 ( $\text{CH}_2 \times 2$ ), 29.6 ( $\text{CH}_2$ ), 29.7 ( $\text{CH}_2$ ), 29.8 ( $\text{CH}_2 \times 7$ ), 32.1 ( $\text{CH}_2$ ), 36.8 ( $\text{CH}_2$ ), 42.7 ( $\text{NCH}_2$ ), 121.5 (q,  $^3J_{\text{C-F}}$  = 4.0 Hz, CH,  $\text{C}_p$ ), 123.3 (q,  $^1J_{\text{C-F}}$  = 274.0 Hz, Cq,  $2\text{CF}_3$ ), 127.8 (q,  $^3J_{\text{C-F}}$  = 3.0 Hz, CH,  $2\text{C}_o$ ), 132.1 (q,  $^2J_{\text{C-F}}$  = 33.3 Hz, Cq,  $2\text{C}_m$ ), 141.4 Cq,  $\text{C}_i$ ), 173.6 (Cq, C=O) ppm. Anal. calcd. for  $\text{C}_{27}\text{H}_{41}\text{F}_6\text{NO}$  (509.30): C, 63.63; H, 8.11; N, 2.75. Found: C, 63.78; H, 8.06; N, 2.79. MS (EI, 70 eV)  $m/z$  (%): 509 (65)  $[\text{M}^+]$ , 466 (16), 354 (34), 340 (36), 284 (100), 243 (61), 227 (13), 174 (15).

#### 4. Conclusions

In summary, we described an operationally simple and sustainable method for the thermal direct amidation of a nonactivated carboxylic acid with amine in the absence of a solvent, catalyst, coupling reagent, and drying agent under normal atmospheric conditions. The releasing of water as the unique by-product gives this approach a remarkable eco-friendly quality. Accomplishing the synthesis of the amide **3** contributed to expanding our previous amide library [27]. The MEP total density showed an electron-rich region around the carbonyl oxygen, whereas an electron-deficient region is located around the amide nitrogen. The frontier molecular orbital energies and global reactivity descriptors showed that the molecule **3** would have a low reactivity owing to its high HOMO–LUMO energy gap (5.54 eV). Besides, the low HOMO energy (−7.38 eV) would indicate the difficulty of electron donation due to its high electronegativity value ( $\chi$  = 4.61 eV). Simulation of the infrared spectrum led to good agreement with the observed spectral patterns. Ultimately, the fatty acid amide **3** could be used as an analog of the endogenous cannabinoid receptor ligand arachidonylethanolamide (anandamide) with potential applications in medicinal chemistry and drug discovery.

**Supplementary Materials:** The following are available online. Figure S1: MS spectrum of the compound **3** (EI technique); Figure S2: IR spectrum of the compound **3** (ATR technique); Figure S3:  $^1\text{H-NMR}$  spectrum of the compound **3**; Figure S4: Expansion  $^1\text{H-NMR}$  spectrum of the compound **3**; Figure S5:  $^{13}\text{C}\{^1\text{H}\}\text{-NMR}$  and DEPT-135 spectra of the compound **3**; Figure S6: Expansion  $^{13}\text{C}\{^1\text{H}\}\text{-NMR}$  and DEPT-135 spectra of the compound **3**; Figure S7: HSQC 2D C–H correlation spectrum of the compound **3**; Figure S8: HMBC 2D C–H correlation spectrum of the compound **3**; Figure S9: Expansion HMBC 2D C–H correlation spectrum of the compound **3**; Figure S10: COSY 2D H–H correlation spectrum of the compound **3**; Figure S11: UV–Vis spectrum of the compound **3**; Figure S12: TLC analysis of amide **3** compared to stearic acid **1** and 3,5-bis(trifluoromethyl)benzylamine **2** using DCM/MeOH (50/1) as mobile phase under UV lamp, 254 nm; Table S1: Atomic coordinates of the optimized structure of **3** calculated at the B3LYP/6-311+G(d,p) level theory in gas phase.

**Author Contributions:** Investigation, data curation, A.S.-T.; writing—review and editing, H.R.; data curation, writing—review and editing, J.J.M.; conceptualization, writing—original draft preparation, D.B.; conceptualization, data curation, writing—original draft preparation, J.-C.C. All authors have read and agreed to the published version of the manuscript.

**Funding:** APC was sponsored by MDPI.

**Institutional Review Board Statement:** Not applicable.

**Informed Consent Statement:** Not applicable.

**Data Availability Statement:** The data presented in this study are available in this article.

**Acknowledgments:** Authors thank to the Dirección de Investigaciones at the Universidad Pedagógica y Tecnológica de Colombia for financial support (project number SGI-3073). We also acknowledge Luis Hurtado and Carlos Rodríguez at the Universidad del Valle for acquiring MS and 1D and 2D NMR spectra and performing elemental analysis. We wish to thank Yeyzon Cruz for acquiring the UV–Vis absorption spectrum.

**Conflicts of Interest:** The authors declare no conflict of interest.

**Sample Availability:** Not available.

## References

1. Pattabiraman, V.; Bode, J. Rethinking amide bond synthesis. *Nature* **2011**, *480*, 471–479. [[CrossRef](#)] [[PubMed](#)]
2. Mahesh, S.; Tang, K.-C.; Raj, M. Amide bond activation of biological molecules. *Molecules* **2018**, *23*, 2615. [[CrossRef](#)]
3. Dunetz, J.R.; Magano, J.; Weisenburger, G.A. Large-scale applications of amide coupling reagents for the synthesis of pharmaceuticals. *Org. Process Res. Dev.* **2016**, *20*, 140–177. [[CrossRef](#)]
4. Bloemendal, V.R.L.J.; Janssen, M.A.C.H.; van Hest, J.C.M.; Rutjes, F.P.J.T. Continuous one-flow multi-step synthesis of active pharmaceutical ingredients. *React. Chem. Eng.* **2020**, *5*, 1186–1197. [[CrossRef](#)]
5. Wang, B.-L.; Zhu, H.-W.; Ma, Y.; Xiong, L.-X.; Li, Y.-Q.; Zhao, Y.; Zhang, J.-F.; Chen, Y.-W.; Zhou, S.; Li, Z.-M. Synthesis, insecticidal activities, and SAR studies of novel pyridylpyrazole acid derivatives based on amide bridge modification of anthranilic diamide insecticides. *J. Agric. Food Chem.* **2013**, *61*, 5483–5493. [[CrossRef](#)]
6. Pereira, E.; Farias, E.; Ribeiro, A.; Alvarenga, E.; Aguiar, A.; Ferreira, J.; Picanço, M. Toxicity of piperine amide analogs toward the tomato pinworm *Tuta absoluta* (Lepidoptera: Gelechiidae) and risk assessment for two predators. *Horticulturae* **2019**, *5*, 70. [[CrossRef](#)]
7. Fayemiwo, K.A.; Chiarasumran, N.; Nabavi, S.A.; Loponov, K.N.; Manović, V.; Benyahia, B.; Vladislavljević, G.T. Eco-friendly fabrication of a highly selective amide-based polymer for CO<sub>2</sub> capture. *Ind. Eng. Chem. Res.* **2019**, *58*, 18160–18167. [[CrossRef](#)]
8. Simplicio, A.L.; Clancy, J.M.; Gilmer, J.F. Prodrugs for amines. *Molecules* **2008**, *13*, 519–547. [[CrossRef](#)] [[PubMed](#)]
9. Bradshaw, P.R.; Wilson, I.D.; Gill, R.U.; Butler, P.J.; Dilworth, C.; Athersuch, T.J. Metabolic hydrolysis of aromatic amides in selected rat, minipig, and human *in vitro* systems. *Sci. Rep.* **2018**, *8*, 2405. [[CrossRef](#)] [[PubMed](#)]
10. Kumari, S.; Carmona, A.V.; Tiwari, A.K.; Trippier, P.C. Amide bond bioisosteres: Strategies, synthesis, and successes. *J. Med. Chem.* **2020**, *63*, 12290–12358. [[CrossRef](#)] [[PubMed](#)]
11. Wodtke, R.; Wodtke, J.; Hauser, S.; Laube, M.; Bauer, D.; Rothe, R.; Neuber, C.; Pietsch, M.; Kopka, K.; Pietsch, J.; et al. Development of an <sup>18</sup>F-labeled irreversible inhibitor of transglutaminase 2 as radiometric tool for quantitative expression profiling in cells and tissues. *J. Med. Chem.* **2021**, *64*, 3462–3478. [[CrossRef](#)]
12. Gisemba, S.A.; Ferracane, M.J.; Murray, T.F.; Aldrich, J.V. Conformational constraint between aromatic residue side chains in the “message” sequence of the peptide arodyn using ring closing metathesis results in a potent and selective kappa opioid receptor antagonist. *J. Med. Chem.* **2021**, *64*, 3153–3164. [[CrossRef](#)] [[PubMed](#)]
13. Chaudhari, P.S.; Salim, S.D.; Sawant, R.V.; Akamanchi, K.G. Sulfated tungstate: A new solid heterogeneous catalyst for amide synthesis. *Green Chem.* **2010**, *12*, 1707–1710. [[CrossRef](#)]
14. Saghatelian, A.; McKinney, M.K.; Bandell, M.; Patapoutian, A.; Cravatt, B.F. A FAAH-regulated class of *N*-acyl taurines that activates TRP ion channels. *Biochemistry* **2006**, *45*, 9007–9015. [[CrossRef](#)] [[PubMed](#)]
15. Devane, W.A.; Hanus, L.; Breuer, A.; Pertwee, R.G.; Stevenson, L.A.; Griffin, G.; Gibson, D.; Mandelbaum, A.; Etinger, A.; Mechoulam, R. Isolation and structure of a brain constituent that binds to the cannabinoid receptor. *Science* **1992**, *258*, 1946–1949. [[CrossRef](#)] [[PubMed](#)]
16. Reggio, P.H. Endocannabinoid binding to the cannabinoid receptors: What is known and what remains unknown. *Curr. Med. Chem.* **2010**, *17*, 1468–1486. [[CrossRef](#)]
17. Huang, S.M.; Bisogno, T.; Petros, T.J.; Chang, S.Y.; Zavitsanos, P.A.; Zipkin, R.E.; Sivakumar, R.; Coop, A.; Maeda, D.Y.; De Petrocellis, L.; et al. Identification of a new class of molecules, the arachidonyl amino acids, and characterization of one member that inhibits pain. *J. Biol. Chem.* **2001**, *276*, 42639–42644. [[CrossRef](#)]
18. Farrell, E.K.; Merkler, D.J. Biosynthesis, degradation, and pharmacological importance of the fatty acid amides. *Drug Discov. Today* **2008**, *13*, 558–568. [[CrossRef](#)]
19. Tripathi, R.K.P. A perspective review on fatty acid amide hydrolase (FAAH) inhibitors as potential therapeutic agents. *Eur. J. Med. Chem.* **2020**, *188*, 111953. [[CrossRef](#)]
20. Singh, S.; Kumar, V.; Sharma, U.; Kumar, N.; Singh, B. Emerging catalytic methods for amide synthesis. *Curr. Org. Synth.* **2013**, *10*, 241–264. [[CrossRef](#)]
21. Lundberg, H.; Tinnis, F.; Selander, N.; Adolfsson, H. Catalytic amide formation from non-activated carboxylic acids and amines. *Chem. Soc. Rev.* **2014**, *43*, 2714–2742. [[CrossRef](#)] [[PubMed](#)]
22. Lukasik, N.; Wagner-Wysiecka, E. A review of amide bond formation in microwave organic synthesis. *Curr. Org. Synth.* **2014**, *11*, 592–604. [[CrossRef](#)]
23. Wang, X. Challenges and outlook for catalytic direct amidation reactions. *Nat. Catal.* **2019**, *2*, 98–102. [[CrossRef](#)]
24. Sabatini, M.T.; Boulton, L.T.; Sneddon, H.F.; Sheppard, T.D. A green chemistry perspective on catalytic amide bond formation. *Nat. Catal.* **2019**, *2*, 10–17. [[CrossRef](#)]
25. Reddy, T.N.; de Lima, D.P. Recent advances in the functionalization of hydrocarbons: Synthesis of amides and its derivatives. *Asian J. Org. Chem.* **2019**, *8*, 1227–1262. [[CrossRef](#)]
26. Massolo, E.; Pirola, M.; Benaglia, M. Amide bond formation strategies: Latest advances on a dateless transformation. *Eur. J. Org. Chem.* **2020**, *2020*, 4641–4651. [[CrossRef](#)]

27. Chaparro, S.; Rojas, H.; Castillo, J.C.; Portilla, J.; Romanelli, G.P.; Pineda, A.; Elsharif, A.M.; Martinez, J.J.; Luque, R. Solventless amide synthesis catalyzed by biogenic CaCO<sub>3</sub> materials. *ACS Sustain. Chem. Eng.* **2020**, *8*, 13139–13146. [[CrossRef](#)]
28. Becerra, D.; Castillo, J.; Insuasty, B.; Cobo, J.; Glidewell, C. Synthesis of *N*-substituted 3-(2-aryl-2-oxoethyl)-3-hydroxy indolin-2-ones and their conversion to *N*-substituted (*E*)-3-(2-aryl-2-oxoethylidene)indolin-2-ones: Synthetic sequence, spectroscopic characterization and structures of four 3-hydroxy compounds and five oxo ethylidene products. *Acta Cryst.* **2020**, *C76*, 433–445. [[CrossRef](#)]
29. Becerra, D.; Rojas, H.; Castillo, J.-C. 3-(*tert*-Butyl)-*N*-(4-methoxybenzyl)-1-methyl-1*H*-pyrazol-5-amine. *Molbank* **2021**, *2021*, M1196. [[CrossRef](#)]
30. Bianchini, G.; Ribelles, P.; Becerra, D.; Ramos, M.T.; Menéndez, J.C. Efficient synthesis of 2-acylquinolines based on an azavinylous Povarov reaction. *Org. Chem. Front.* **2016**, *3*, 412–422. [[CrossRef](#)]
31. Acosta, P.; Becerra, D.; Gouedranche, S.; Quiroga, J.; Constantieux, T.; Bonne, D.; Rodriguez, R. Exploiting the reactivity of 1,2-ketoamides: Enantioselective synthesis of functionalized pyrrolidines and pyrrolo-1,4-benzodiazepine-2,5-diones. *Synlett* **2015**, *26*, 1591–1595. [[CrossRef](#)]
32. Castillo, J.-C.; Orrego-Hernández, J.; Portilla, J. Cs<sub>2</sub>CO<sub>3</sub>-Promoted direct *N*-alkylation: Highly chemoselective synthesis of *N*-alkylated benzylamines and anilines. *Eur. J. Org. Chem.* **2016**, *2016*, 3824–3835. [[CrossRef](#)]
33. Abonia, R.; Castillo, J.C.; Garay, A.; Insuasty, B.; Quiroga, J.; Nogueras, M.; Cobo, J.; D’Vries, R. A facile synthesis of stable β-amino-*N*-/*O*-hemiacetals through a catalyst-free three-component Mannich-type reaction. *Tetrahedron Lett.* **2017**, *58*, 1490–1494. [[CrossRef](#)]
34. Becke, A.D. Density-functional thermochemistry. III. The role of exact exchange. *J. Chem. Phys.* **1993**, *98*, 5648–5652. [[CrossRef](#)]
35. Lee, C.; Yang, W.; Parr, R.G. Development of the Colle-Salvetti correlation-energy formula into a functional of the electron density. *Phys. Rev.* **1988**, *37B*, 785–789. [[CrossRef](#)] [[PubMed](#)]
36. Glover, S.A.; Rosser, A.A. Heteroatom substitution at amide nitrogen-resonance reduction and HERON reactions of anomeric amides. *Molecules* **2018**, *23*, 2834. [[CrossRef](#)] [[PubMed](#)]
37. Antonijevic, I.S.; Janjic, G.V.; Milcic, M.; Zaric, S.D. Preferred geometries and energies of sulfur–sulfur interactions in crystal structures. *Cryst. Growth Des.* **2016**, *16*, 632–639. [[CrossRef](#)]
38. Nataraj, A.; Balachandran, V.; Karthick, T. Molecular orbital studies (hardness, chemical potential, electrophilicity, and first electron excitation), vibrational investigation and theoretical NBO analysis of 2-hydroxy-5-bromobenzaldehyde by density functional method. *J. Mol. Struct.* **2013**, *1031*, 221–233. [[CrossRef](#)]
39. Politzer, P.; Abu-Awwad, F. A comparative analysis of Hartree-Fock and Kohn-Sham orbital energies. *Theor. Chem. Acc.* **1998**, *99*, 83–87. [[CrossRef](#)]
40. Parr, R.G.; von Szentpaly, L.; Liu, S. Electrophilicity index. *J. Am. Chem. Soc.* **1999**, *121*, 1922–1924. [[CrossRef](#)]
41. Frisch, M.J.; Trucks, G.W.; Schlegel, H.B.; Scuseria, G.E.; Robb, M.A.; Cheeseman, J.R.; Scalmani, G.; Barone, V.; Petersson, G.A.; Nakatsuji, H.; et al. *Gaussian 16 Revision B.01*; Gaussian, Inc.: Wallingford, CT, USA, 2019.